ELSEVIER

Polymer donor–polymer acceptor (all-polymer) solar cells

Antonio Facchetti

Department of Chemistry, Northwestern University and Polyera Corporation, USA

Organic photovoltaic (OPV) cells represent an exciting class of renewable energy technology; they are lightweight and flexible, and have a low production cost. Over the last two decades, the efficiency of these devices has improved significantly, in particular through the development of solution-processed bulk heterojunction (BHJ) OPV cells. While fullerenes have been the most intensively studied acceptor materials in BHJ OPVs, research is currently underway in several groups investigating non-fullerene molecular acceptors. In this review, initial breakthroughs and recent progress in the development of polymer donor-polymer acceptor (all-polymer) BHJ OPVs are highlighted.

Introduction

Organic photovoltaic (OPV) cells are a revolutionary technology for electrical energy production, being inexpensive to fabricate, lightweight, and mechanically flexible [1–7]. Initial OPV devices based on a vapor-deposited donor–acceptor small-molecule heterojunction exhibited a power conversion efficiency (PCE) of ~1% (Fig. 1a). However, during the last two decades dramatic performance increases have been achieved [8–12], particularly through the development of solution-processed bulk heterojunction (BHJ) OPV devices (Fig. 1B) [13–15]. In a typical BHJ OPV cell, the photoactive blend layer, comprising a conjugated polymer donor and a soluble molecular acceptor [16,17] is sandwiched between an indium tin oxide (ITO) electrode (anode) and a metal electrode (cathode). The polymer donor serves as the main solar light absorber and as the hole transporting phase, whereas the small molecule transports electrons [18]. Therefore a wide optical absorption range (to match the solar spectrum), large extinction coefficients, and large carrier mobilities are basic requirements toward the design of ideal photoactive blends. Furthermore, microstructural features favoring light-to-charge and charge transport in the out-of-plane direction are essential characteristics to enhance charge collection.

Fullerenes [19,20], particularly $PC_{60}BM$ (Fig. 1) [21] and its C70-based homologue [22], have been the most investigated acceptors in BHJ OPVs and utilized to improve the polymer donor design rules [23,24], better understand/optimize fabrication processes, and enhance active layer morphology [25–28]. There are several reasons for the supremacy of fullerenes in this field, including favorable LUMO energy, reversible electrochemical reduction [29], excellent electron transport characteristics [30], and anisotropic charge transport [31]. Following recent developments of high-performance electron-transporting materials for organic field-effect transistors [32], several research groups have begun investigating non-fullerene molecular acceptors for BHJ OPVs with recent exciting results [33]. However, progress in polymer donor-polymer acceptor (all-polymer) OPVs remains behind recent achievements for small molecule-polymer blends. This review will highlight initial breakthroughs and recent progress in the development of all-polymer BHJ OPVs.

Basics principles and operation of organic solar cells

Typical BHJ OPV cells are shown schematically in Fig. 1 along with the energetic levels involved in charge generation/transport (Fig. 1d). In these devices, a glass or plastic substrate is coated with a thin layer of high work function ITO functioning as the transparent anode. The photoactive layer is sandwiched between the anode and the top low work function cathode, typically Al or Ca. Interfacial layers can be inserted between the anode-photoactive and cathode-photoactive layers to improve device performance and stabilize operation [34]. For efficient operation the photoactive blend should produce an interpenetrating network of donor and acceptor domains, with considerable interfacial area and effective percolation pathways connecting the acceptor regions to the cathode and donor regions to the anode (Fig. 2).

E-mail address: a-facchetti@northwestern.edu.

1369-7021/06/$ - see front matter http://dx.doi.org/10.1016/j.mattod.2013.04.005

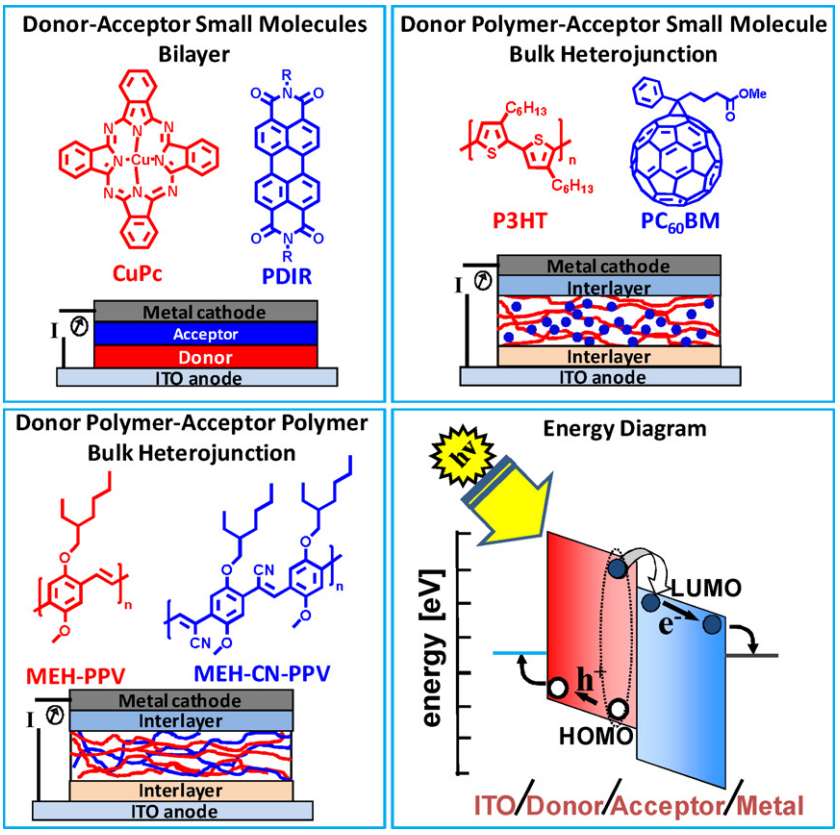

FIGURE 1

Structure and representative photoactive materials of (top left) a single heterojunction, (top right) polymer-donor–molecular acceptor and (bottom left) all-polymer bulk heterojunction photovoltaic cells. (Bottom right) Energy levels of the materials where light absorption/excitation dissociation/charge collection takes place.

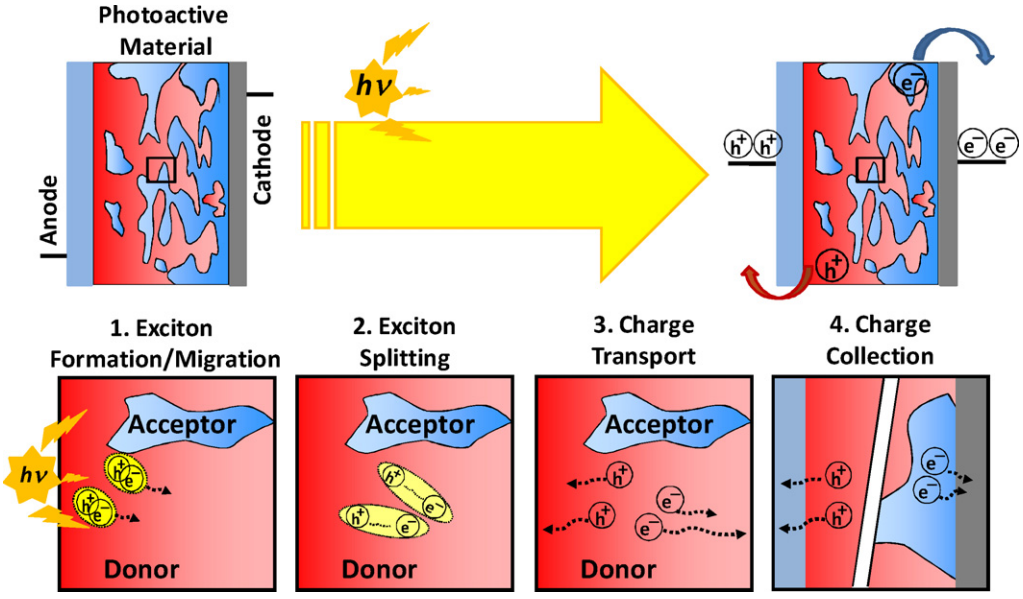

FIGURE 2

(Top) Schematic of a BHJ OPV cell showing energy production upon illumination. (Bottom) The four key processes converting solar energy (photons) into electrical energy (charge flow).

Several key processes must be optimized for efficient operation (Fig. 2) including [35]: (1) light absorption to create hole–electron pairs (excitons); (2) exciton diffusion to the donor–acceptor interface and splitting to free carriers; (3) migration of holes (in the donor) and electrons (in the acceptor) toward the contacts for collection due to the built-in electric potential/field. A key difference between organic and conventional inorganic cells is the exciton binding energy, which is much smaller for Si (~0.1 eV)

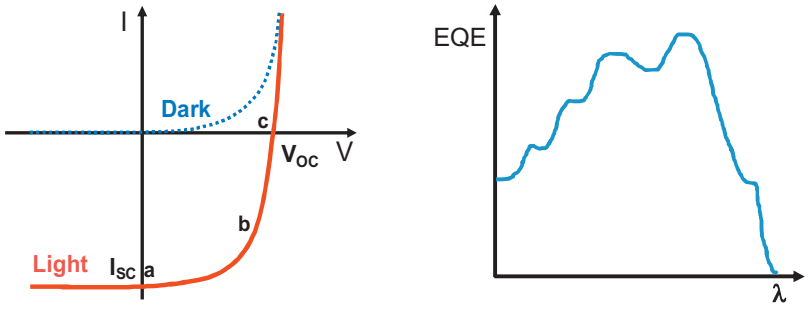

FIGURE 3

(Left) *I–V* curve in the dark (blue) and under illumination (red). (Right) EQE versus wavelength for an OPV cell.

than for typical organic semiconductors (~0.5 eV). Thus, excitons only split at the photoactive materials interface in an OPV; (4) charge collection at the electrodes. Other OPV processes to take into account include exciton quenching, charge recombination, and charge leakage.

Fig. 3 shows typical OPV current (*I*) (or current density, *J*) versus voltage (*V*) plots in the dark and under illumination, and the energy levels involved. In the dark, the *I–V* curve passes through the origin but under illumination, the *I–V* curve shifts downward, resulting in electrical current. Such plots are used to evaluate device performance parameters including: (1) the open-circuit voltage (V_{oc}, the cell voltage in sunlight when no current is flowing); (2) the short-circuit current (I_{sc}, the current flowing through an illuminated cell when there is no external resistance); (3) the fill factor (FF; the ratio of actual maximum power output to theoretical power output if both current and voltage are maximum, I_{sc} and V_{oc}, respectively); (4) the PCE, the ratio of power output to power input; (5) the external quantum efficiency (EQE, the device efficiency as a function of the energy or incident radiation wavelength). From the photocurrent spectrum the ability of the solar cells to convert photons to electrons under irradiation at certain wavelengths and intensities can be obtained. The overall PCE is calculated according to the following equations:

$$\eta = \frac{P_{out}}{P_{in}} = \frac{\mathrm{FF}(V_{oc}I_{sc})}{P_{in}} \quad (1)$$

$$\mathrm{FF} = \frac{V_{mpp}I_{mpp}}{V_{oc}I_{sc}} \quad (2)$$

where P_{out} is the maximum output electrical power of the device under illumination and P_{in} is the light intensity incident on the device.

To achieve cells with large PCE and stability, the materials have to be designed carefully to tune HOMO/LUMO energy levels, solar light absorption, and blend morphology/microstructure [36] as well as transport characteristics [37]. The material absorption intensity plays a critical role, and in fullerene-based cells, it is typically fulfilled by the donor. The photogenerated excitons must then migrate to the D/A interface. This depends on the exciton diffusion length, which for most organic materials is on the order of tens of nm [38]. Once the exciton reaches the interface, charge transfer must occur. In this case, the driving force to move the electron from the LUMO of the donor to the LUMO of the acceptor must be on the order of the exciton binding energy –a few tenths of a volt – requiring some energetic offset between the LUMO energies of the donor and acceptor species. This description lays out the basic electronic structure characteristics that must be designed into the individual donor and acceptor materials. Along with the obvious photostability and electrochemical requirements, the acceptor must have a LUMO energy when compared to the donor HOMO to yield a large voltage, yet the acceptor LUMO must also be sufficiently below the donor LUMO to allow efficient electron transfer. In the case of polymers with very small HOMO–LUMO gaps, this tuning of the acceptor LUMO can be a delicate task.

All-polymer photoactive blends

All-polymer OPVs, in which an *n*-type semiconducting polymer is used as the electron acceptor instead of a fullerene [39–41] or another small molecule [42] have some unique advantages: (1) semiconducting polymers have high absorption coefficients in the visible spectral region, while fullerenes are limited. Although C70 derivatives are better than C60s [43,44], it is quite difficult to extend their absorption into the red and near-infrared regions. (2) Polymer energy level can be tuned more efficiently. A low-lying acceptor LUMO can result in more efficient photoinduced charge separation at the donor/acceptor interfaces, but it may reduce the V_{oc}. (3) Polymer-polymer blends offer superior flexibility in controlling solution viscosity, an important factor for large scale OPV module production by solution processes. In the following sections, I will summarize selected combinations of polymer donor (Fig. 4)–polymer acceptor (Fig. 5) blends for OPV, and the reader should refer to these figures to access the polymers' structures. For easy of discussion, these blends are described based on the structural feature of the acceptor.

Cyanated polyphenylenevinylenes

Conjugated polymers based on cyanated poly(phenylenevinylene) (PPV, Table 1) backbones (Fig. 4) were the first investigated independently by Friend [45] and Heeger [46]. By using the BHJ approach, both teams demonstrated that photogenerated excitons in the polymer layer can be efficiently dissociated into free carriers at the photoactive blend interface. Friend used a mixture of two PPV polymers, donor MEH-PPV and acceptor C6-CN-PPV to fabricate cells and investigated details of blend phase segregation using TEM, STEM, and parallel electron-energy-loss spectroscopy (PEELS). Interestingly, the authors used $FeCl_3$ to selectively oxidize (dope) MEH-PPV throughout the film thickness making it possible to image and differentiate the acceptor vs. the donor polymer domains. Evidence of photoluminescence quenching was also clearly provided. These devices exhibited a strong photoresponse with a V_{oc} of 0.6 V and EQEs of up to 6%, which increase substantially to 15% and 40% at reverse biases of 3.5 and 10 V. These

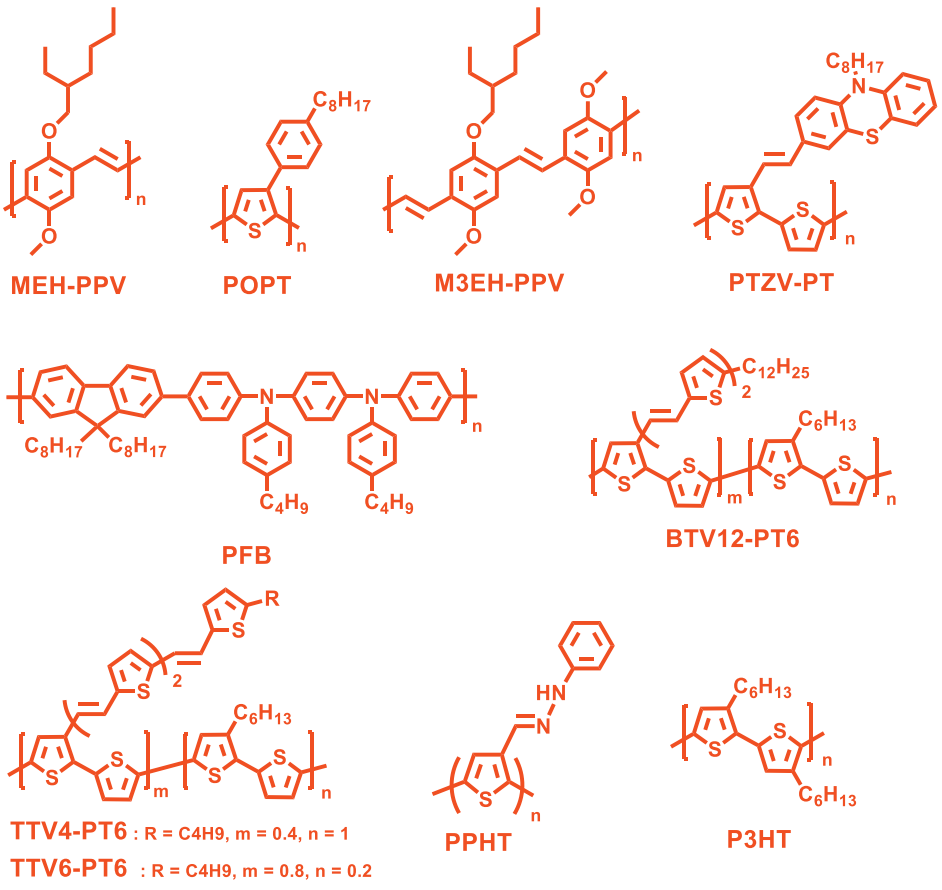

FIGURE 4

Chemical structure of selected donor polymers used in all-polymer blends for BHJ solar cells.

performances were far greater than those measured for MEH-PPV (0.04%) and C8-CN-PPV (~10^{-3}%) films alone. In a parallel study, Heeger observed similar phenomena using the same donor polymer but using MEH-CN-PPV as the acceptor. The absorption and photoluminescent spectra from films of MEH-PPV, CN-PPV, and CN-PPV:MEH-PPV blends indicated no ground-state charge transfer but only photoinduced charge transfer. OPV devices were based on ITO-glass substrates and Ca or Al metals as the cathode. The blend devices exhibited EQEs of ~5% and PCEs of ~0.9% (V_{oc} = 1.25 V), which were 15–25× and 100× larger than in photodiodes fabricated with pure MEH-PPV and MEH-CN-PPV, respectively.

The polymeric acceptor MEH-CN-PPV was also investigated with donor POPT [47–54] to fabricate laminated devices [55] exhibiting the largest PCEs of that time. Interestingly, while the simple laminated devices with the pure polymer in each of the two layers exhibited low efficiencies, by adding 2–5 wt% of POPT to the MEH-CN-PPV layer (and vice versa), the device efficiency increased considerably compared to the double layer device (or single-layer blend). OPV performances were maximized for devices of type Au/PEDOT/[POPT:MEH-CN-PPV (19:1)]/[MEH-CNPPV:POPT (19:1)]/Ca, in which the EQE reached 29% at 480 nm excitation and no applied bias. The PCE was 1.9% with FF ~30–35%. More recently Frechet *et al.* [56] synthesized the donor polymer POPT via GRIM resulting in a high M_n and regioregular polymer which afforded PCEs of 3.1% with $PC_{61}BM$. More importantly, thanks to the high solvent resistance of GRIM POPT, bilayer devices with MEH-CN-PPV afforded PCEs of 2.0% (V_{oc} ~ 1 V, J_{sc} ~ 5.5 mA/cm^2, FF < 50%) [57,58].

Carter and co-workers [59] investigated M3EH-PPV (donor)/CN-ether-PPV (acceptor) blends versus the donor-only devices and varied the polymer layer thickness and device electrodes to understand efficiency evolution. Single polymer devices using M3EH-PPV yielded PCEs of 0.40% using a TiO_2/polymer/Au configuration, while blends of M3EH-PPV and CN-ether-PPV afforded 0.75% efficiencies for the same electrodes and 1.0% for PEDOT and Ca electrodes. Kietzke *et al.* [60] also investigated M3EHPPV:CN-ether-PPV blends in more details and compared the performance of the polymer blend versus the two-layer devices. Before this study, despite the lower probability for excitons to reach the interface, the highest polymer-polymer PCEs were achieved for double-layer OPVs. Cells were fabricated on ITO/PEDOT:PSS on which the blend solution in chlorobenzene was spin-coated, and then completed by evaporating Ca/Al electrodes. The authors proposed that due to the much lower solubility of M3EH-PPV in chlorobenzene compared to CN-ether-PPV, not a homogeneous blend but rather a vertically composition graded layer is formed during spin coating. This led to a nearly ideal blend structure facilitating both exciton separation and efficient charge transport. Thus, cells prepared from M3EH-PPV/CN-ether-PPV blends yielded very high PCEs of up to 1.7% (V_{oc} = 1.36 V, FF = 35%, I_{sc} = 3.54 mA) vs. 1.3% (V_{oc} = 1.31 V, FF = 32%, I_{sc} = 3.12 mA) for the corresponding bilayer devices. More recently the same team used solvents with different boiling points and solvent mixtures to

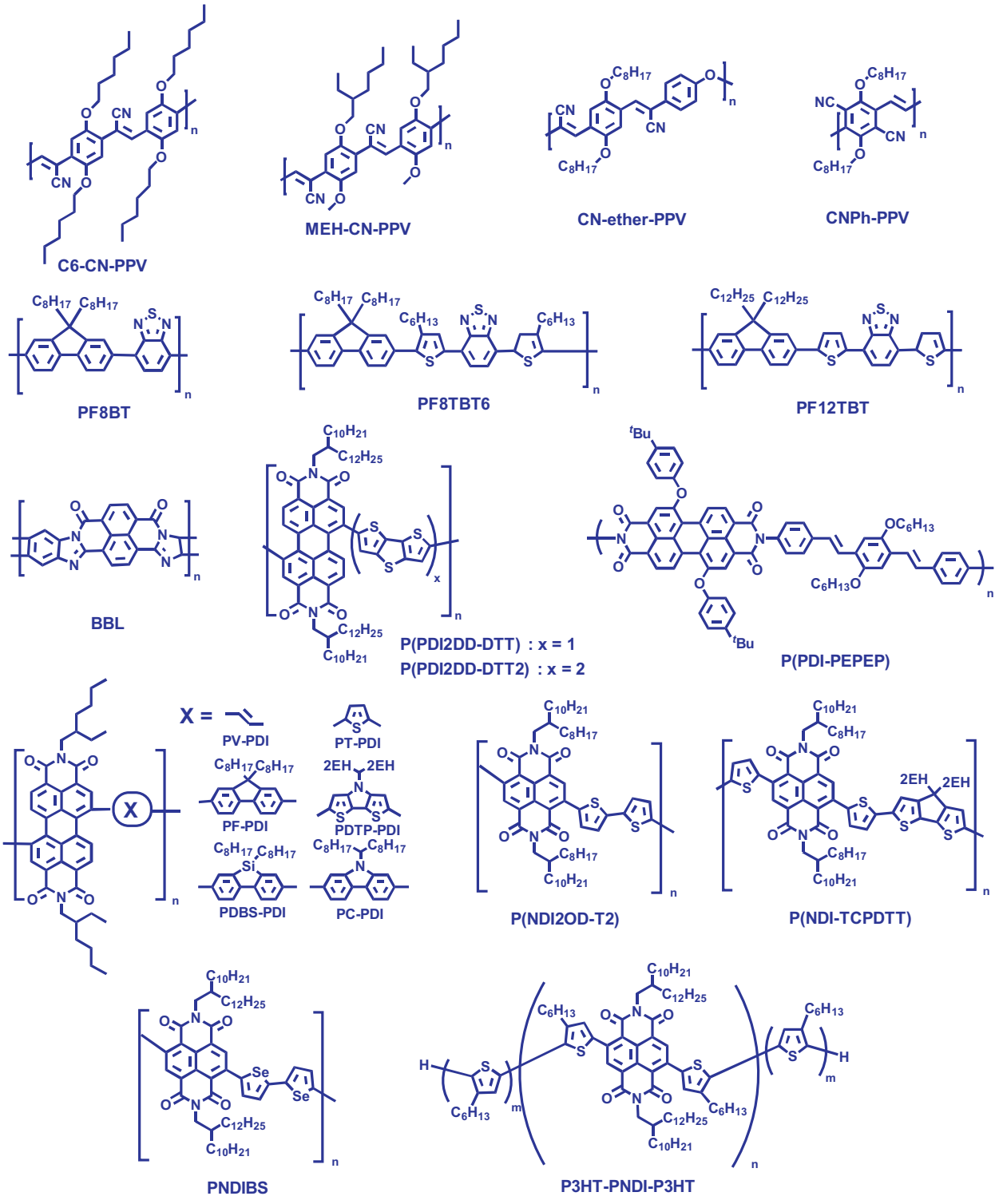

FIGURE 5

Chemical structure of selected acceptor polymers used in all-polymer blends for BHJ solar cells.

tune the blend morphology and investigated the photophysics in more details [61].

Li *et al.* reported cells based on PTZV-PT as donor and CNPh-PPV as the acceptor [62]. The HOMO/LUMO levels of PTZV-PT are 4.99/2.99 eV, thus higher than those of CNPh-PPV (5.75/3.65 eV) corroborating the observed fluorescence quenching. PTZV-PT exhibits a broad absorption plateau extending from 350 to 650 nm while the absorption spectrum of CNPh-PPV covers a relatively narrower wavelength range (from 400 to 590 nm). OPV devices were annealed at different temperatures to optimize the performance. ITO/PEDOT:PSS/blend(1:1)/LiF/Al without thermal treatment exhibits a PCE of ~0.41% (V_{oc} = 0.75 V, J_{sc} = 2.02 mA cm^{-2}, FF = 27%). After blend annealing at 120 °C for 15 min, the V_{oc} increased to 0.85 V, the J_{sc} increased to 3.14 mA cm^{-2}, and the FF

TABLE 1

Photoactive blend composition and device performance for solar cells based on cyanated polyphenylenevinylenes[a]

Donor	Acceptor	Blend (D:A)	Device structure	V_{oc}/V (FF/%)	PCE (EQE/%)	Ref
MEH-PPV	C6-CN-PPV	7:1 and 1:10	ITO/blend/Ca or Al	0.6	(6)[b]	[45]
MEH-PPV	MEH-CN-PPV	1:1	ITO/blend/Ca or Al	1.25	0.25–0.9 (1–6)[c]	[46]
POPT	MEH-CN-PPV	Laminated	Au/PEDOT/laminate/Ca or Al	~1.1 (30–35)	1.9 (29)	[55]
POPT via GRIM	MEH-CN-PPV	Bilayer	ITO/PEDOT/bilayer/Al	~1 (<50)	2.0	[57,58]
M3EH-PPV	CN-ether-PPV	1:1	ITOPEDOT/blend/Ca	1 (25)	1.0	[59]
M3EH-PPV	CN-ether-PPV	1:1	ITO/PEDOT/blend/Ca/Al	1.36 (35)	1.7 (~30)	[60]
Phenothiazine	CNPh-PPV	1:1	ITO/PEDOT/blend/LiF/Al	0.85 (29)	0.8	[62]

[a] Performance values were measured at AM 1.5 and 100 mW/cm^2 unless indicated. EQE is the maximum value.
[b] Measured at 550 nm and 0.15 mW/cm^2.
[c] Measured at 430 nm, from 20 mW/cm^2 to ~1 μ W/cm^2.

was 28.8%, thus giving an overall PCE of 0.8%. The low FFs was an indication of a rather unbalanced charge transport.

Benzothiadiazole-based polymers

A key class of electron-poor polymers for OPV are those based on the strong electron width-drawing benzothiadiazole heterocycle (Table 2). Arias *et al.* [63] first investigated the phase separation and photovoltaic properties of PF8BT in combination with the donor polymer PFB. PF8BT is a highly luminescent polymer with a high electron affinity (3.53 eV) whereas PFB is a triarylamine-based hole transporting polymer. Polymer blends were deposited by spin-coating or drop-casting from chloroform or xylene. From AFM it was found that the use of volatile chloroform prevents significant rearrangement of the polymer chains resulting in a fine phase separation. In addition, PFB:PF8BT films prepared by spin-coating from chloroform show charge separation quenching of the photoluminescence to a level of 3.7%. This result indicates that excitons were very efficiently dissociated in the blend, thus PFB and PF8BT are phase-separated on a scale similar to the exciton diffusion length. Consequently, devices fabricated from chloroform showed an EQE of 4% at 3.2 eV excitation whereas devices made by spin-coating from xylene showed an EQE of 1.8%. In contrast, films prepared by drop-casting showed phase separation on a much larger scale as shown by the AFM topography images. Furthermore fluorescence microscopy images indicated that the higher phase observed by AFM corresponds to a PF8BT-emitting phase. However, photoluminescence efficiency measurements show that even in films with apparent in-plane phase separation on a length scale of tens of microns, the PL is significantly reduced. Indeed, the PL efficiency of a pure PF8BT film is 58%, while the PL efficiency of a PFB:PF8BT blend prepared by drop-casting is reduced considerably to 18%. This cannot be accounted for by the relatively small interfacial area between the two polymer phases. Thus, this result suggested that the distinct phases observed through microscopy were not pure. The high PL quenching, and therefore the high probability of exciton dissociation in the spin-coated films from chloroform are in agreement with the higher photovoltaic efficiencies observed for these devices. However, the maximum EQE for the spin-coated devices was greater than that of the drop-cast devices by only 2×. This weaker dependence of the photovoltaic efficiency on feature size compared to the dependence of the PL quenching, along with the AFM and fluorescence microscopy, suggested that a tradeoff exists between optimized charge separation and transport in these blends. In a successive study, Friend [64] used the same polymers and found that the photoluminescence quenching is insensitive to the blend composition but the photovoltaic response is strongly composition dependent. MacNeill and coworkers [65] used the same blend to quantitatively map the composition using scanning transmission X-ray microscopy (STXM).

TABLE 2

Photoactive blend composition and device performance for solar cells based on benzothiadiazole polymers[a]

Donor	Acceptor	Blend	Structure	V_{oc}/V (FF/%)	PCE (EQE/%)	Ref
PFB	PF8BT	1:1	ITO/blend/Al		(2–4)[b]	[63]
PFB	PF8BT	500:1 to 1:500	ITO/PEDOT/blend/Metal		(0.2–4)[c]	[64]
P3HT	PF8BT	6:4	ITO/PEDOT/blend/LiF/Al	0.4–0.5 (30–40)	0.13 (~1.5)	[66]
P3HT	PF8TBT6	1:1	ITO/PEDOT/blend/LiF/Al		1.8 (25)	[67]
P3HT	PF8TBT6	Nanoimprint	ITO/PEDOT/NI/LiF/Al	1.14 (49)	1.85 (26)	[68]
P3HT	PF8BT	1:1	ITO/PEDOT/blend/Al	0.69–0.98	(5–20)	[69]
P3HT	PF8TBT6	1:1	ITO/PEDOT/blend/Al	1.0–1.2	(3–6)	[69]
P3HT	PF12TBT	1:1	ITO/PEDOT/blend/LiF/Al	1.19 (42)	2.0	[70]

[a] Performance values were measured at AM 1.5 and 100 mW/cm^2 unless indicated. EQE is the maximum value.
[b] Measured at 3.2 eV at 0.1 mW/cm^2.
[c] Measured at 335, 400, 480 nm, power not reported.

Bradley and co-workers [66] employed the same acceptor (PF8BT) but P3HT as the donor polymer. Several fabrication parameters were investigated to optimize OPV efficiencies including the blend composition, film thickness, solvent type, and the use of LiF as interlayer. The highest EQEs and PCEs were achieved for the blend with 60 wt% P3HT using p-xylene as a solvent. Insertion of a LiF layer was found to improve the PCE from 0.02% to 0.13%. To understand the poor efficiency, this polymer blend system was analyzed in relation to charge separation efficiency, time-of-flight charge carrier mobility, and charge recombination dynamics, measured by transient absorption spectroscopy. The results showed that the poor electron mobility of PF8BT is mainly responsible for the low efficiency. OPVs using PF8TBT6 both as electron acceptor, in blends with P3HT, and as hole acceptor, in blends with $PC_{60}MB$ were also investigated [67]. This work also demonstrated that efficient ambipolar transport in polymers is achieved for charge carrier densities much lower than is the case for FETs. ITO/PEDOT:PSS/blend(70–80 nm)/Al devices based on 1:1 weight ratio PF8TBT6/P3HT blends exhibit maximum EQE of 26%. For optimized PF8TBT6/P3HT devices incorporating LiF/Al electrodes, PCEs of 1.8% were measured. Furthermore, the same polymer blend was studied by Friend and Huck *et al.* [68] by a completely new approach to nanopatter the blends through nanoimprint lithography (NIL). A clear improvement in the PCE of the nanostructured devices was observed for the 25 nm features leading to a PCE of 1.85%, which is 50% higher than the blend control devices.

MacNeill [69] used blends of P3HT with both PF8TBT6 and PF8BT to compare the evolution of photophysical properties and device performance with thermal annealing (form <100 °C to >200 °C). In blends with PF8TBT6, P3HT was found to reorganize at low annealing temperatures (<100 °C), evidenced by a redshift of both absorption and photoluminescence (PL), and by decreased PL lifetime. Annealing to 140 °C, however, was found to optimize device performance (EQE max ~ 20%), accompanied by an increase in PL efficiency and lifetime. Grazing-incidence small-angle X-ray scattering was performed to study the film nanomorphology evolution with annealing. It was concluded that reorganization of P3HT alone is not sufficient to optimize device performance but must also be accompanied by a coarsening of the morphology to promote charge separation. In contrast to blends with PF8TBT6, P3HT is only found to reorganize in blends with F8BT at annealing temperatures of over 200 °C. The low efficiency of the P3HT:F8BT system (EQE max ~ 6%) was attributed to poor charge generation and separation resulting from the failure of P3HT to reorganize. Finally, Miyake [70] used PF12TBT with P3HT to fabricate cells using different solvents. In structures ITO/PEDOT:PSS/blend/LiF/Al, PCEs as high as 2.0% were achieved with chloroform, with J_{sc} up to 4 mA cm^2 and V_{oc} of 1.19, and FF of ~42%. To address the origin of the different device performances depending on the spin-coating solvents, the authors measured atomic force microscopy phase images of P3HT/PF12TBT blend films before and after thermal annealing.

Perylene- and naphthalenediimide-based polymers

OPV cells incorporating rylene diimide-based acceptor polymers were developed more recently but they are among the most efficient among all-polymer solar cells. Note that we will not discuss structurally similar, yet not rylene-based, polymers (e.g. BBL) discovered by Jeneky and co-workers despite their interesting properties [71]. Studies on rylene diimide begun with the work of Marder [72] using P(PDI2DD-DTT) as the acceptor. The HOMO/LUMO energies of P(PDI2DD-DTT) were estimated at 3.9/5.9 eV by electrochemistry. Thin film of P(PDI2DD-DTT) showed significant absorption throughout the visible and extending into the near-IR region. OPV cells were fabricated using BTV-PT in a structure of ITO/PEDOT:PSS/blend(1:1, w/w)/Al. This blend exhibits a very broad absorption between 250 and 850 nm, a maximum EQE of 44% at 540 nm, and PCEs > 1% (V_{oc} = 0.63 V, J_{sc} = 4.2 mA/cm^2, FF = 39%). Later, the same group investigated OPVs based on related donor (PT1) and acceptor P(PDI2DD-DTT2) blends and achieved PCEs as high as 1.5% (V_{oc} = 0.69 V, J_{sc} = 5.02 mA/cm^2, FF = 43%) [73]. Using an alternating PDI-phenylenevinylene copolymer (P(PDI-PEPEP)) acceptor and poly(3-phenyl hydrazone thiophene) (PPHT) donor in OPVs, Mikroyannidis *et al.* obtained a PCE of 2.3% under white-light illumination calibrated to an AM1.5 intensity of 30 mW cm^{-2}, after annealing at 80 °C for 10 min [74].

A very comprehensive study on PDI-based acceptor polymer blends was carried out very recently by Hashimoto [75]. The authors synthesized several X-PDI-based co-polymers (X-PDI) including those having as X the co-monomers vinylene (V), thiophene (T), dithienopyrrole (DTP), fluorene (F), dibenzosilole (DBS), and carbazole (C). P3HT and PT1 were used as donors. The LUMO energy levels of these polymers were estimated by electrochemistry and varied from 4.05 eV for PV–PDI to 3.61 eV for PF–PDI whereas the donor HOMOs are 5.08 eV for PT1 and 4.91 eV for P3HT. OPV cells with structure glass/ITO/PEDOT:PSS/blend/Ca/Al were investigated. The data showed that the devices based on the PT1/PX–PDI blends had higher V_{oc} (0.58–0.76 V) than those of the devices based on the P3HT/PX–PDI blends (0.44–0.58 V). This result is in agreement with the LUMO(A)–HOMO(D) values. At the same time, the PT1/PX–PDI blends also showed higher J_{sc} than their corresponding P3HT/PC–PDI blends. When using chloroform as solvent the PCEs of these polymers ranged from 0.1 to 0.3% when using P3HT and 0.5–1.1% when using PT1 as the donor. Performance optimization was carried out for the best acceptor, PC-PDI, by varying the solvent. The greatest PCE of 2.23% for PT1-PC-PDI was achieved using a solvent mixture of toluene/chloroform 9:1 (Table 3).

Recently, our laboratory has developed a new class of copolymers based on naphthalenediimide (NDI) for optoelectronics [76], with P(NDI2OD-T2) being the most investigated [77]. Electron mobility measurements in top-gate organic field effect transistor (OFET) structures yielded large electron mobility of 0.85 $cm^2\ V^{-1}\ s^{-1}$, while the analysis of the space charge limited current in electron-only devices and time-of-flight measurements yielded remarkable values for the bulk mobility of $>10^{-3}\ cm^2\ V^{-1}\ s^{-1}$ [78]. Structural investigations regarding the origin of the exceptional high electron mobility in P(NDI2OD-T2) revealed a significant degree of thin-film crystallinity [79], which directly affects its bulk charge transport properties [80]. Loi *et al.* first demonstrated that P(NDI2OD-T2)/P3HT blends form a type-II heterojunction, resulting in photogenerated charges accessed by time resolved photoluminescence measurements [81]. Furthermore, high performance ambipolar FETs with balanced electron ($4 \times 10^{-3}\ cm^2$/V) and hole ($2 \times 10^{-3}\ cm^2$/V) mobilities were achieved. Loi and co-workers also first reported the photovoltaic properties of the polymer-blend thin films [82].

TABLE 3

Photoactive blend composition and device performance for solar cells based on perylene- and naphthalenediimide polymers[a]

Donor	Acceptor	Blend	Structure	V_{oc}/*V* (FF/%)	PCE (EQE/%)	Ref
BTV12-PT6	P(PDI2DD-DTT)	1:1	ITO/PEDOT/blend/Al	0.63 (39)	>1	[72]
TTV4-PT6	P(PDI2DD-DTT2)	1:3	ITO/PEDOT:PSS/blend/Ca/Al	0.69 (43)	1.5	[73]
PPHT	P(PDI-PEPEP)	1:1	ITO/blend/Al	0.60 (39)	2.3[b]	[74]
TTV6-PT6	X-PDI	2:1	ITO/PEDOT:PSS/blend/Ca/Al	0.58–0.76 (38–49)	0.5–1.1	[75]
P3HT	X-PDI	2:1	ITO/PEDOT:PSS/blend/Ca/Al	0.44–0.58 (46–58)	0.1–0.3	[75]
TTV6-PT6	PC-PDI	2:1	ITO/PEDOT:PSS/blend/Ca/Al	0.7 (50)	2.23 (~45)	[75]
P3HT	P(NDI2OD-T2)	1:2 (CB)	ITO/PEDOT:PSS/blend/cathode	0.55 (70)	0.16	[82,84]
P3HT	P(NDI2OD-T2)	1:2 (Xylene)	ITO/PEDOT:PSS/blend/Ca/Al	0.49 (54)	0.62	[82]
P3HT	P(NDI2OD-T2)	1:0.75	ITO/PEDOT:PSS/blend/Sm/Al	0.56 (65)	1.4 (23)	[86]
P3HT	P(NDI-TCPDTT)	1:1.5	ITO/PEDOT:PSS/blend/Sm/Al	0.63 (70)	1.1 (15)	[86]
P3HT	PNDIBS	1:3	ITO/PEDOT:PSS/blend/LiF/Al	0.53 (44)	0.88	[87]
P3HT	P3HT-PNBI-P3HT	1:1	ITO/PEDOT:PSS/blend/Ca/Al	0.56 (50)	1.28	[88]
PV1013	P(NDI2OD-T2)	1:1	ITO/ZnO/blend/V_2O_5/Al	4.0–4.2 (52)	0.79 (45)	[89]

[a] Performance values were measured at AM 1.5 and 100 mW/cm^2 unless indicated. EQE is the maximum value.
[b] Measured at 1.15 Sun (30 mW/cm^2).

The devices were fabricated on PEDOT:PSS-coated ITO substrates with LiF/Al electrodes and where the blend (1:1 and 1:2) P3HT/P(NDI2OD-T2 weight ratio) was spun from both from chlorobenzene or dichlorobenzene. Enhanced photovoltaic performances were observed when the P(NDI2OD-T2) concentration in the polymer-blend is increased. The observed open circuit voltage ~0.5 eV is consistent with the $HOMO_D$–$LUMO_A$ difference expected from the energy level offset of P3HT and P(NDI2OD-T2). Interestingly, the FF values of these devices were very large (~70%), suggesting high charge separation efficiency and balanced carrier mobility, in agreement with the ambipolar FET data. Despite these favorable charge transport conditions, the devices exhibit modest short-circuit current densities (J_{sc} = 0.34–0.49 mA/cm^2), resulting in very low power conversion efficiencies (PCE = 0.09–0.16%). To understand if recombination processes were limiting the device performance, light intensity dependent measurements on the most efficient devices were carried out, and the data suggested that major charge carrier losses are due to monomolecular (exciton or geminate pair) and not bimolecular recombination. Thus, blend morphology was investigated by AFM and it was found that a vertically phase-separated structure of the blends is formed upon chlorobenzene evaporation, with a P(NDI2OD-T2) rich phase on the top of the thin films. In a bilayer-like structure only a narrow layer near to the planar heterojunction is involved in the photovoltaic process, strongly limiting the devices performance. To improve the lateral (vs. horizontal) blend phase separation, xylene was used as solvent. Self-assembly of P3HT occurs readily in xylene, leading to whisker-like nanostructures that increase the bulk D/A interface along the thin films with the formation of charge percolation pathways. The resulting PCEs improved to 0.28–0.62% (1:1 to 1:2, w/w D/A blends) with V_{oc} = 0.49–0.48 V, FF = 54%, J_{sc} = 1.02–2.39 mA/cm^2. In a related paper, Loo and co-workers also investigated P(NDI2OD-T2) in combination with P3HT/P(NDI2OD-T2) blend for laminated cells to understand morphology variations at the buried interface [83].

In parallel, Sirringhaus *et al*. studied in details the morphology, device physics and photophysics of P3HT-P(NDI2OD-T2) blends to further rationalize why despite P(NDI2OD-T2) high electron mobility, deep LUMO and near infrared absorption band the corresponding solar cells perform poorly [84]. In their study a maximum PCE of 0.2% was achieved in line with the abovementioned studies and confirmed a morphological dependence of the device efficiency. To investigate bulk film morphology, scanning transmission X-ray microscopy (STXM) were performed for the first time for this blend. Interestingly, the AFM-derived surface topography of the films do not match well with the morphology revealed by STXM, highlighting the limits of AFM in revealing information about bulk phase separation. In order to probe blend excited state dynamics and facilitate identification of loss mechanisms which may limit cell PCEs, the authors used femtosecond- and nanosecond transient absorption (TA) measurements. Despite the fast and efficient charge formation as indicated by the broadening of the PIA band in the first ~20 ps and the PL quenching measurement, the transient absorption (TA) kinetics show a strong decrease in the PIA signal over the first ~200 ps. This decay was assigned to sub-nanosecond recombination of charge-pairs, similar, but much faster and having a greater magnitude than that found for P3HT:PF8TBT6 blends [85].

Neher *et al.* [86] investigated the electronic structure and morphology of two NDI-based acceptors, P(NDI2OD-T2) and P(NDI-TCPDTT), in combination with P3HT. Their investigation clearly demonstrated that NDI-based device performance is strongly enhanced when preventing the polymers to form large and well-ordered crystallites in the blend layer. By combining optical spectroscopy and morphological investigations, the authors demonstrated that an optimal nanomorphology is obtained by suppressing NDI polymer aggregation at the early stage of film formation. To investigate how P(NDI2OD-T2) solution aggregation affect performance, the degree of pre-aggregation was tuned by going from a strongly collapsed, hence aggregated chain conformation (as in pure p-xylene) to a more coiled or aggregate-free

conformation (as in pure cyanonaphthalene). The pure p-xylene device show a high fill factor (FF = 61%) but low PCE (0.24%) and limited J_{sc} of 0.8 mA/cm^2 (V_{oc} = 0.47 V). The addition of cyanonaphthalene resulted in a marked performance improvement with the best PCE of 1.4% achieved for a 1:1 p-xylene:cyanonaphthalene mixture (FF = 65%, V_{oc} = 0.56 V). For the P3HT:P(NDI-TCPDTT) blend, an improvement in device performance was observed when adding cyanonaphthalene to p-xylene, but the effect was far weaker than for P(NDI2OD-T2)-based blends, which was attributed to the lower tendency of P(NDI-TCPDTT) to pre-aggregate in solution. The best cells were obtained using tetraline as solvent and exhibited a PCE of 1.1% (FF = 70%, V_{oc} = 0.63 V, J_{sc} = 2.43 mA/cm^2). Very recently, an NDI polymer where dithiophene is replaced by diselenophene (PNDIBS) was reported by Jeneky *et al.* [87] and showed PCEs of ~0.9% in blends with P3HT. Also, Mori *et al.* used [88] a fully conjugated block copolymer P3HT-PNBI-P3HT and blend with P3HT (1:1 by weight) exhibited PCEs of 1.28%, V_{oc} of 0.56 V, J_{sc} of 4.57 mA/cm^2, and FF of 50%. Finally, our team very recently reported that using P(NDI2OD-T2) with a finely tuned donor polymer (Polyera ActivInk PV1013), an efficiency as large as 4.2% can be achieved [89]. This data is mainly the result of the enhanced current density (~10 mA/cm^2) and the V_{oc} (0.79 V) as the FF is lower than those obtained for other blends using this acceptor. Thus, the latest results strongly suggest that the NDI-based family has great potential for further development.

Conclusions

From the discussion in the previous section it is clear that performances of all polymer OPV cells do not yet compete with those of polymer donor/molecular acceptor devices. The origin of this efficiency discrepancy has often been attributed to the lower electron mobility of most conjugated polymers compared to fullerenes, and inappropriate electronic coupling between the donor/acceptor components. However, several electron-transporting polymers now exhibit very large electron mobilities. Other negative factors are related to un-optimized thin-film blend morphology, including large phase separation, inhomogeneous internal phase composition, and reduced ordering of polymer chains, as well as large geminate charge recombination [90,91]. Since polymeric acceptor-based solar cells are actually polymer–polymer cells (the donor is always a polymer), optimization of device performance relies upon an understanding and control of the morphology and the phase-separation processes of polymer blends [92]. Another important aspect of optimizing polymer–polymer cells has been having tools to structurally characterize the photoactive blend. Performance optimization will eventually rely on the development of new acceptor polymers and a better pair of donor–acceptor materials [93–96]. To date, far less polymeric acceptors have been synthesized when compared to the donor counterpart. However, momentum toward the development of new electron-depleted building blocks is increased due to the recent promising results in electron-transporting materials for OLED, OLETs, and OTFTs. Furthermore, the recent first certified all-polymer cell demonstrated by the Polyera Corporation team (Fig. 6) [97,98], achieving PCE > 5% (and more recently >6%) [99,100], indicates that there are no fundamental reasons as why all-polymer blends cannot achieve efficiencies of fullerene-polymer devices. Thus, with increased synthetic efforts dedicated toward the design of

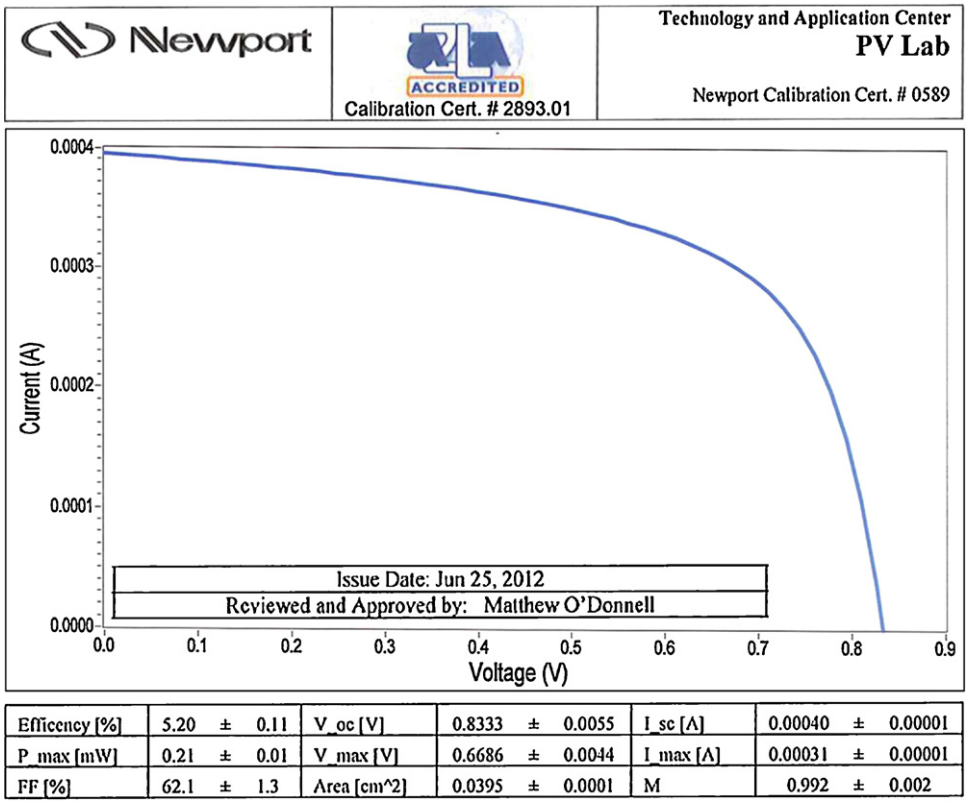

FIGURE 6

First certified all-polymer blend solar cell achieving a PCE of 5.2% fabricated at Polyera Corporation and certified by Newport.

efficient donor/acceptor polymer combinations, polymer/polymer-blend photovoltaic devices have the potential to contribute significantly toward improving state-of-the-art in OPVs and paving the way to all-polymer OPV panels [101].

References

[1] C. Piliego, M.A. Loi, J. Mater. Chem. 22 (10) (2012) 4141.
[2] A. Facchetti, Chem. Mater. 23 (3) (2011) 733.
[3] N.A.D. Yamamoto, et al. J. Phys. Chem. C 116 (35) (2012) 18641.
[4] W.-Y. Wong, B.Z. Tang, Macromol. Chem. Phys. 211 (23) (2010) 2460.
[5] C.W. Tang, Appl. Phys. Lett. 48 (1986) 183.
[6] W.C. Tsoi, et al. ACS Nano 6 (11) (2012) 9646.
[7] D. Gendron, M. Leclerc, Energy Environ. Sci. 4 (4) (2011) 1225.
[8] G. Yu, et al. Science 270 (1995) 1789.
[9] S. Gunes, H.S. Neugebauer, N.S. Sariciftci, Chem. Rev. 107 (2007) 1324.
[10] K. Coakley, M.D. McGehee, Chem. Mater. 16 (2004) 4533.
[11] C. Li, et al. Chem. Rev. 110 (2010) 6817.
[12] F. Silvestri, A. Marrocchi, Int. J. Mol. Sci. 11 (2010) 1471.
[13] F. Zhang, et al. J. Mater. Chem. 21 (44) (2011) 17590.
[14] C.L. Chochos, S.A. Choulis, Prog. Polym. Sci. 36 (10) (2011) 1326.
[15] H. Zhou, L. Yang, W. You, Macromolecules 45 (2) (2012) 607.
[16] C.J. Brabec, N.S. Sariciftci, J.C. Hummelen, Adv. Funct. Mater. 11 (2001) 15.
[17] B.C. Thompson, J.M. Frechet, J. Angew. Chem., Int. Ed. 47 (2008) 58.
[18] Y. Li, Y. Zou, Adv. Mater. 20 (2008) 2952.
[19] E.M. Perez, Pure Appl. Chem. 83 (1) (2011) 201.
[20] G. Dennler, M.C. Scharber, C.J. Brabec, Adv. Mater 21 (2009) 1323, and references therein.
[21] J.C. Hummelen, et al. J. Org. Chem. 60 (1995) 532.
[22] M.M. Wienk, et al. J. Angew. Chem., Int. Ed. 42 (2003) 3371.
[23] N.M. O'Boyle, C.M. Campbell, G.R. Hutchison, J. Phys. Chem. C 115 (32) (2011) 16200.
[24] M.C. Scharber, et al. Adv. Mater. 18 (2006) 789.
[25] N. Stingelin, Polym. Int. 61 (6) (2012) 866.
[26] F.C. Jamieson, et al. Chem. Sci. 3 (2) (2012) 485.
[27] J.K. Lee, et al. J. Am. Chem. Soc. 130 (2008) 3619.
[28] L.-M. Chen, et al. Adv. Mater. 21 (2009) 1434.
[29] Q. Xie, W. Perez-Cordero, L.J. Echegoyen, Am. Chem. Soc. 114 (1992) 3978.
[30] P.H. Wobkenberg, et al. Synth. Met. 158 (2008) 468.
[31] N.C. Cates, et al. Nano Lett. 9 (2009) 4153.
[32] Y. Wen, Y. Liu, Adv. Mater. 22 (2010) 1331.
[33] J.E. Anthony, Chem. Mater. 23 (2011) 583.
[34] P.J. Hotchkiss, et al. Acc. Chem. Res. 45 (3) (2012) 337.
[35] C.W. Schlenker, M.E. Thompson, Chem. Commun. 47 (13) (2011) 3702.
[36] M. O'Neill, S.M. Kelly, Adv. Mater. 23 (5) (2011) 566.
[37] C.J. Brabec, et al. Chem. Soc. Rev. 40 (3) (2011) 1185.
[38] O.V. Mikhnenko, et al. Energy Environ. Sci. 5 (2012) 6960.
[39] F. Giacalone, N. Martin, Adv. Mater. 22 (2010) 4220.
[40] F. Wuerthner, K. Meerholz, Chem. Eur. J. 16 (2010) 9366.
[41] O. Inganaes, et al. Adv. Mater. 22 (2010) E100.
[42] J.E. Anthony, et al. Adv. Mater. 22 (2010) 3876.
[43] T. Umeyama, H. Imahori, J. Phys. Chem. C 117 (2013) 3195–3209.
[44] C.-Z. Li, H.-L. Yip, K.-Y. Jen Alex, J. Mater. Chem. 22 (2012) 4161–4177.
[45] J.J.M. Halls, et al. Nature 376 (1995) 498–500.
[46] G. Yu, A.J. Heeger, J. Appl. Phys. 78 (1995) 4510–4515.
[47] M.R. Andersson, et al. Macromolecules 27 (1994) 6503.
[48] Q. Pei, et al. Macromolecules 25 (1992) 4297.
[49] T. Johansson, et al. J. Mater. Chem. 13 (2003) 1316.
[50] A. Gadisa, et al. Appl. Phys. Lett. 84 (2004) 1609.
[51] D.M. deLeeuw, et al. Synth. Met. 87 (1997) 53.
[52] K.E. Aasmundtveit, et al. Macromolecules 33 (2000) 5481.
[53] M.R. Andersson, et al. Macromolecules 28 (1995) 7525.
[54] M. Theander, et al. J. Phys. Chem. B 103 (1999) 7771.
[55] M. Granstrom, et al. Nature 395 (1998) 257.
[56] T.W. Holcombe, et al. J. Am. Chem. Soc. 131 (2009) 14160.
[57] T. Kietzke, H. Horhold, D. Neher, Chem. Mater. 17 (2005) 6532.
[58] S.A. Jenekhe, S. Yi, Appl. Phys. Lett. 77 (2000) 2635.
[59] A.J. Breeze, et al. Sol. Energy Mater. Sol. Cells 83 (2004) 263.
[60] T. Kietzke, H.-H. Horhold, D. Neher, Chem. Mater. 17 (2005) 6532.
[61] C. Yin, et al. J. Phys. Chem. C 112 (2008) 14607.
[62] G. Sang, et al. Appl. Phys. Lett. 94 (2009) 193302.
[63] A.C. Arias, et al. Macromolecules 34 (2001) 6005.
[64] H.J. Snaith, et al. Nano Lett. 2 (2002) 1353–1357.
[65] C.R. McNeill, et al. Macromolecules 40 (2007) 3263–3270.
[66] Y. Kim, et al. Chem. Mater. 16 (2004) 4812–4818.
[67] C.R. McNeill, et al. Appl. Phys. Lett. 90 (2007) 193506.
[68] X. He, et al. Nano Lett. 10 (2010) 1302.
[69] C.R. McNeill, et al. Adv. Funct. Mater. 19 (2009) 3103–3111.
[70] D. Mori, et al. ACS Appl. Mater. Interfaces 3 (8) (2011) 2924.
[71] M.M. Alam, S.A. Jenekhe, Chem. Mater. 16 (2004) 4647.
[72] X. Zhan, et al. J. Am. Chem. Soc. 129 (2007) 7246.
[73] Z.A. Tan, et al. Appl. Phys. Lett. 93 (2008) 073309.
[74] J.A. Mikroyannidis, et al. J. Phys. Chem. C 113 (2009) 7904.
[75] E.N. Zhou, et al. Angew. Chem. Int. Ed. 50 (2011) 2799.
[76] X.W. Zhan, et al. Adv. Mater. 23 (2011) 268.
[77] H. Yan, et al. Nature 457 (2009) 679.
[78] R. Steyrleuthner, et al. Adv. Mater. 22 (2010) 2799.
[79] J. Rivnay, et al. Adv. Mater. 22 (2010) 4359.
[80] J. Rivnay, et al. Macromolecules 44 (2011) 5246.
[81] K. Szendrei, et al. J. Mater. Chem. 20 (2010) 1317.
[82] S. Fabiano, et al. J. Mater. Chem. 21 (2011) 5891.
[83] J. Kim, et al. Chem. Mater. (2010) 4931.
[84] J.R. Moore, et al. Adv. Energy Mater. 1 (2011) 230.
[85] M. Hodgkiss, et al. Phys. Rev. Lett. 104 (2010) 177701.
[86] M. Schubert, et al. Adv. Energy Mater. 2 (2012) 369–380.
[87] Y.-J. Hwang, et al. Macromolecules (2012), http://dx.doi.org/10.1021/ma3020239.
[88] K. Nakabayashi, H. Mori, Macromolecules (2012), http://dx.doi.org/10.1021/ma302170e.
[89] A. Facchetti, Presented at the Organic Photovoltaics XIII Symposium, SPIE Optics + Photonics Annual Meeting, San Diego, USA, 2012.
[90] M.M. Mandoc, et al. J. Appl. Phys. 101 (2007) 104512.
[91] C. Yin, et al. Appl. Phys. Lett. 90 (2007) 092117.
[92] R. Steyrleuthner, et al. J. Am. Chem. Soc. 134 (2012) 18303.
[93] J.D. Azoulay, et al. Macromolecules 46 (4) (2013) 1337.
[94] Y.-W. Su, S.-C. Lan, K.-H. Wei, Mater. Today 15 (12) (2012) 554–562.
[95] H. Mori, et al. Org. Electron. 13 (10) (2012) 1975.
[96] I. Osaka, et al. ACS Macro Lett. 1 (4) (2012) 437.
[97] http://www.mmdnewswire.com/polyera-all-polymer-organic-solar-cells-117704.html.
[98] A. Facchetti, Presented at the 3rd Conference on Organic Photovoltaics, Würzburg, Germany, 2012.
[99] During the proof revision of this review, NERL certified a Polyera all-polymer cell at 6.4%. See: www.polyera.com.
[100] A. Facchetti Presented at the Hybrid and Organic Photovoltaic Conference, Sevilla, Spain 2013.
[101] D.J. Lipomi, Z. Bao, Energy Environ. Sci. 4 (9) (2011) 3314.